Impact of Interfaces on Photoluminescence Efficiency of High-Indium-Content (In, Ga)N Quantum Wells

P. Wolny,[1,*] H. Turski,[1] G. Muziol,[1] M. Sawicka,[1] J. Smalc-Koziorowska,[1] J. Moneta,[1] M. Hajdel,[1] A. Feduniewicz-Żmuda,[1] S. Grzanka,[1] R. Kudrawiec,[2] and C. Skierbiszewski[1]

[1] *Institute of High Pressure Physics, Polish Academy of Sciences, Warsaw 01-142, Poland*

[2] *Department of Semiconductor Materials Engineering, Wrocław University of Science and Technology, Wybrzeże Wyspiańskiego 27, 50-370 Wrocław, Poland*

(Received 28 June 2022; revised 26 September 2022; accepted 23 November 2022; published 17 January 2023)

(In, Ga)N-based light-emitting diodes (LEDs) are known to suffer from low electron-hole wave-function overlap due to a high piezoelectric field. Staggered (In, Ga)N quantum wells (QWs) are proposed to increase the wave-function overlap and improve the efficiency of LEDs, especially for long-wavelength emitters. In this work, we show evidence that the growth of staggered QWs by plasma-assisted molecular beam epitaxy has another beneficial effect, as it allows a reduction in the formation of defects, responsible for nonradiative Shockley-Read-Hall recombination, at the bottom interface of the QW. Staggered QWs comprised an (In, Ga)N layer of an intermediate In content between the barrier and the QW. We show that insertion of such a layer results in a significant increase of the luminescence intensity, even if the calculated wave-function overlap drops. We study the dependence of the thickness of such an intermediate-In-content layer on photoluminescence intensity behavior. Staggered QWs exhibit increased cathodoluminescence homogeneity that is a fingerprint of a lower density of defects, in contrast to standard QWs for which a high density of dark spots is observed in QW-emission mapping. Transmission electron microscopy of standard QWs reveals the formation of basal-plane stacking faults and voids that can result from vacancy aggregation. A stepwise increase of the In content in staggered QWs prevents the formation of point defects and results in an increased luminescence efficiency. The In-composition difference between the barrier and the well is, therefore, a key parameter to control the formation of point defects in the high-In-content QWs, influencing the luminescence efficiency. Characteristics of the cyan laser diode (LD) utilizing staggered QWs are presented.

DOI: 10.1103/PhysRevApplied.19.014044

I. INTRODUCTION

The fabrication of nitride-based emitters still poses a challenge when long emission wavelengths in the green part of the spectrum are considered. There are two main reasons for the existence of the so-called "green gap." The first is a consequence of the presence of large electric fields in GaN/(In, Ga)N quantum wells (QWs), which separate the free carriers and decrease the wave-function overlap [1,2]. Especially for high-indium-content QWs, the built-in electric field can significantly decrease the quantum efficiency of nitride structures, due to the decrease of the electron-hole wave-function overlap. The second reason is related to more challenging (In, Ga)N epitaxy, leading to defect formation [3,4]. The optimization of the structural and optical quality of (In, Ga)N QWs addresses the thermodynamic and structural limitations, i.e., overcoming the high decomposition rate of In—N bonds while preserving the high optical quality of high-In-content (In, Ga)N [5–7]. Additionally, proper strain engineering is required to control the large lattice mismatch in high-indium-content QWs to avoid the generation of misfit defects [8,9].

The impact of the growth conditions on the quantum efficiency (QE) is also important for blue light-emitting diodes (LEDs). We would like to point out that an increase of the QE in blue LEDs by introducing the (In, Ga)N interlayer before the QWs for metal-organic vapor-phase epitaxy (MOVPE) growth was recently discussed very intensively [10,11]. According to one of the hypotheses, the QE collapse can been ascribed to the generation of surface defects (vacancies) in GaN at high growth temperatures, which are then trapped by (In, Ga)N QWs [10]. The other report indicates unintentional doping to be the reason for the presence of nonradiative recombination centers [11]. As an explanation, in both cases, the (In, Ga)N

*wolny@unipress.waw.pl

interlayer is important to bury these defects (vacancies or impurities) before the QW is grown.

The concept of staggered QWs has been utilized for green emitters for quite some time already. Originally, it was proposed in order to increase the electron-hole wave-function overlap [12,13]. Interestingly, in the LED structures grown by MOVPE, the enhancement in electroluminescence from LEDs with staggered QWs is larger than that predicted theoretically. However, the authors speculate only on the reason for it, mentioning (1) more-pronounced carrier screening that reduces energy-band bending and further increases overlap of Γ_{e-hh}, (2) improved material quality, and (3) better carrier confinement in the staggered (In, Ga)N QWs.

Here, we discuss the origin of the increased photoluminescence (PL) of staggered (In, Ga)N QWs grown by plasma-assisted molecular beam epitaxy (PAMBE) with respect to their standard counterparts. The behavior of PL is investigated by taking into account two effects: (1) electron-hole wave-function overlap and (2) the generation of extended and point defects (vacancies) at the interface between the barrier and QW. Our study presents a comparison of standard and staggered QWs. We show that the insertion of an (In, Ga)N layer of an intermediate In content (which we call a pre-QW) just before the QW has a beneficial effect on the luminescence efficiency of the staggered QW. The increase in the luminescence intensity observed in staggered QWs can be attributed to a reduced density of defects, which is due the smaller difference in composition at (In, Ga)N interfaces in comparison with standard QWs. We propose that defects which reduce PL intensity are related to the generation of a large number of vacancies when standard high-In-content (In, Ga)N QWs are grown. An additional argument supporting vacancies being generated at the interface between (In, Ga)N layers that greatly differ in In content is the fact that vacancy aggregation can result in basal-plane stacking faults (BSFs) and void formation [14]. The presence of such defects is confirmed experimentally by transmission electron microscopy (TEM). Note that the introduction of a pre-QW is proposed to improve the luminescence intensity of MBE-grown high-In-content QWs emitting in 480–512 nm wavelengths (cyan-green). For blue QWs with an In composition of 17%, a pre-QW is not needed. Moreover, the proposed approach should not be confused with the concept of (In, Ga)N or (In, Al)N underlayers applied in MOCVD-grown structures to bury the defects and grow GaN over them. The idea presented in this work involves the insertion of a very thin layer (from 0.2 to 5 nm) just before the QW of an intermediate composition. We note that the density of defects formed at the bottom interface of a QW can be reduced for structures with pre-QWs (but is not fully eliminated, especially when the In content in QW increases from 22 to 24%).

II. EXPERIMENT

The QW structures studied here are grown by PAMBE in a custom-designed Gen20A reactor (Veeco Instruments). High-N flux is a key factor to obtain high-In-content (In, Ga)N layers without decreasing the growth temperature [5,15]. Therefore, our MBE reactor is equipped with three cryopumps, providing unusually high pumping speed, which are required to maintain the conditions of noninteracting atomic beams during epitaxy with high-N fluxes. Typical N flux during MBE growth is about 0.3 μm/h, while, for the growth of high-In-content (In, Ga)N, the N flux is increased to 2.8 μm/h, as expressed in equivalent growth units of GaN (0001). Bulk GaN substrates with a threading-dislocation density of 1×10^7 cm^{-2} are used. Indium-rich growth conditions are employed to ensure the step-flow surface morphology at a growth temperature of 650 °C [16]. The presence of indium on the surface after growth and the growth temperature are monitored by laser reflectometry [17]. The (In, Ga)N growth conditions needed to obtain a specific In content are calibrated separately on another set of samples for which the In content is assessed by x-ray diffraction. The photoluminescence is measured at room temperature with a continuous-wave (CW) He-Cd laser operating at $\lambda = 325$ nm and a pulse Nd : YAG laser operating at $\lambda = 266$ nm in 1-ns pulses with a 1-kHz repetition rate. The excitation power density of the CW is about 50 W/cm^2. While for pulse measurements, the maximum power density is 145 kW/cm^2. Conventional high-resolution TEM, high-angle annular dark-field (HAADF) scanning TEM (STEM), and quasi-bright-field (BF) STEM using a HAADF detector with a long camera length (1.8 m) are performed on an FEI TITAN 200 transmission electron microscope operated at 200 keV in cross section for the selected samples.

Details of all the structures discussed in this work are listed in Table I. Three series of samples are grown. In each of the series, two types of structures are grown: standard (without pre-QWs) and staggered (with pre-QWs). The first and second series consist of double 2.6-nm (In, Ga)N QWs with an In content of 22% and 24%, respectively. The third series consists of a single 12-nm (In, Ga)N QW with an In content of 22%. Samples with thin QWs contain two QWs, while samples with wide QWs have only a single QW. Schematic diagrams of the composition profiles in the thin double QWs and wide single QW are presented in Figs. 1(a) and 1(b), respectively. Pre-QW thickness is denoted as d. Note that, for $d = 0$, there is no pre-QW. The thickness of the pre-QW (In, Ga)N layer is varied from 0 to 5 nm in the third series of samples with wide QWs. The In content in the (In, Ga)N barriers between the QWs and cap layer is the same in all of the samples and equal to 8%. The In composition of 8% in (In, Ga)N

TABLE I. List of samples studied with the thicknesses of pre-QW and QW indicated. The electron-hole wave-function overlaps are numerically calculated for single QWs for a given QW and pre-QW thickness. Room-temperature PL maximum wavelength is presented together with the relative intensity.

Sample	Number of QWs	Pre-QW d (nm)	QW (nm)	$\langle\Psi_e\|\Psi_h\rangle$ at $j = 100$ A/cm^2	Room-temperature PL: QW peak wavelength (nm)	Room-temperature PL: Intensity (% of the reference)
*A*0	2	0	2.6	0.40	491	22
*A*1	2	1	2.6	0.33	488	56
*B*0	2	0	2.6	0.38	512	4
*B*1	2	1	2.6	0.32	512	13
*W*0	1	0	12	0.45[a]	479	1
*W*02	1	0.2	12	0.42[a]	475	74
*W*1	1	1	12	0.35[a]	480	100
*W*2	1	2	12	0.38[a]	480	92
*W*5	1	5	12	0.47[a]	478	92

[a]For wide QWs, the values are only given for the most probable transition.

barriers is used to match a typical waveguide composition in our MBE-grown lasers. Such laser diodes (LDs) with (In, Ga)N waveguides benefit from a higher optical confinement [18,19]. All structures used in this study are nominally undoped.

The In content in the pre-QW layer is 16%. Table I also presents the maximum peak position and relative intensity of room-temperature PL, as well as electron-hole wave-function overlaps numerically calculated for single QWs for given QW and pre-QW thicknesses.

III. RESULTS AND DISCUSSION

A. Photoluminescence studies

The room-temperature PL spectra of the three sample pairs are shown in Figs. 2(a)–2(c). The first pair, *A*0-*A*1, constitute double-QW structures that have 22% In in the (In, Ga)N QW (2.6 nm thickness) and emit at about 490 nm. Sample *A*0 has a standard abrupt composition profile of QWs ($d = 0$ nm), while, in sample *A*1, each QW is preceded by the 1-nm-thick pre-QW (In, Ga)N layer with an In composition of 16%. A similar sample pair is represented by *B*0 and *B*1 (QW thickness of 2.6 nm), but here the In content of the QWs is 24%, which results in a longer emission wavelength with the peak maximum at 512 nm. The last sample pair is *W*0 and *W*1, which represents the results for single 12-nm-thick QWs of 22% In, emitting at 480 nm. The PL spectrum of each sample is measured under identical conditions. For all three pairs of samples, we observe a higher emission intensity for the staggered structure, regardless of the QW's In content or width. The external quantum efficiency (EQE) versus excitation power density for all samples with thinner wells, *A*0, *A*1, *B*0, and *B*1, are shown in Fig. 2(d). The presented EQEs are calculated as the ratio of integrated spectra to excitation power density. It can be deduced that for sample *A*1

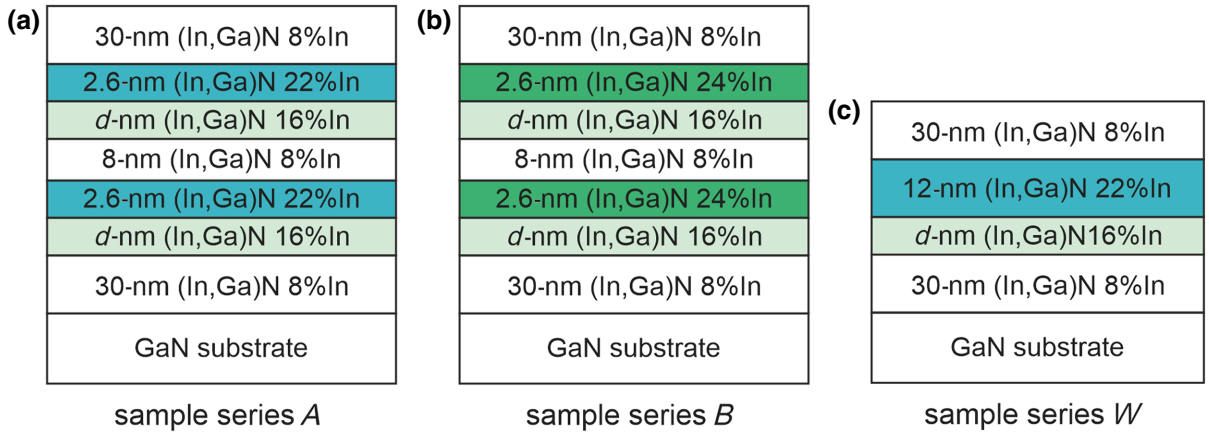

FIG. 1. Schematic diagram presenting the studied QW structures that comprise pre-QWs of thickness d inserted before (a),(b) 2.6-nm-thick double QWs and (c) 12-nm-thick single QW.

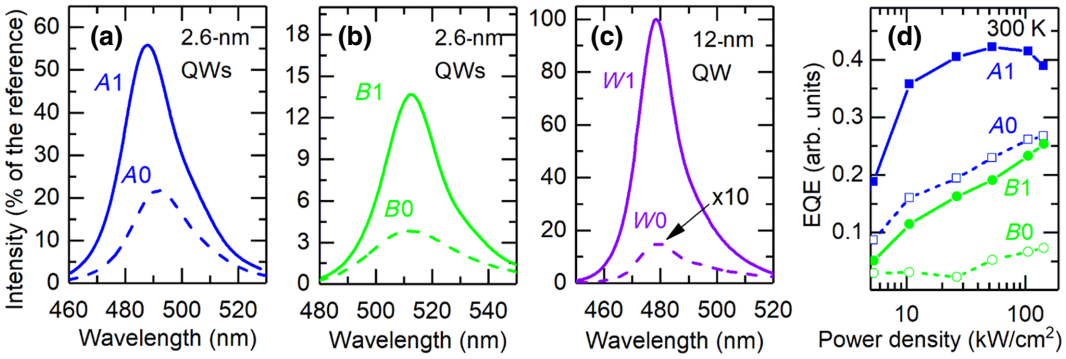

FIG. 2. Comparison of RT PL of staggered and standard QWs: double QW structures with 2.6-nm-thick QWs having (a) 22% In and (b) 24% In in the QWs and (c) 12-nm-thick single QW with 22% In content. PL of standard structures and staggered structures with a pre-QW thickness of 1 nm are presented as dashed and solid lines, respectively. (d) Relative EQE versus pulsed excitation power density on a logarithmic scale for samples $A0$, $A1$, $B0$, and $B1$.

the maximum EQE is around 50–70 kW/cm^2. For all other measured samples, the EQE increases with increasing excitation power. This is evidence that the CW PL results presented in Fig. 2(a)–2(c) fall in the Shockley-Reed-Hall regime of the EQE dependence, i.e., are dominated by nonradiative-recombination processes involving defects.

The impact of the insertion of the pre-QW on the electron-hole (e-h) wave-function overlaps, $\langle\psi_e|\psi_h\rangle$, is verified theoretically. Energy-band structures and electron and hole wave functions are calculated for all the structures under study using SiLENSe 6.4 [20]. To simulate the band structures with and without excitation, we place the QW structure in a p-n junction to allow for carrier injection. On the n side 200-nm GaN:Si and on the p side 200-nm GaN:Mg are added; the doping in both layers is set to 4×10^{18} cm^{-3}. First, the bias in the simulations is set to 2.6 V. Under such conditions, the electric field from the p-n junction is entirely screened, while, at the same time, the current density is small ($j < 10^{-5}$ A/cm^2). We use this picture as an approximation of the situation of the $A1$ and $W1$ QWs without excitation. Next, the thin and wide QWs are compared under excitation. We choose a current density equal to $j = 100$ A/cm^2. This current density is an order of magnitude higher than that used in LEDs and an order of magnitude lower than that used in LDs.

Single QWs 2.6 and 12 nm thick, with or without a pre-QW, are considered. It is worth mentioning that, in the case of 12-nm-thick QWs, the wave-function overlap between the ground states is negligible; however, under excitation, there is a transition path through the excited states, which can probably be exceptionally high [21]. The applicability of wide QWs is confirmed by implementing them into laser-diode structures [21,22]. In the case of 12-nm-wide QWs, there are several transitions that can participate in carrier recombination. However, for the purpose of this work, we restrict ourselves to a qualitative comparison, presenting only the highest $\langle\psi_e|\psi_h\rangle$ value for the respective structures in Table I. Furthermore, despite the e-h wave-function overlaps being calculated for a single QW, the results still well illustrate the experimentally studied structures with two QWs ($A0$, $A1$ and $B0$, $B1$) that are far apart. One can see that $\langle\psi_e|\psi_h\rangle$ in thin QWs with a pre-QW are, in fact, lower than the standard QWs. This is a consequence of the fact that the total QW thickness increases significantly after insertion of the pre-QW layer. Such an effect is not so clearly visible for a wide

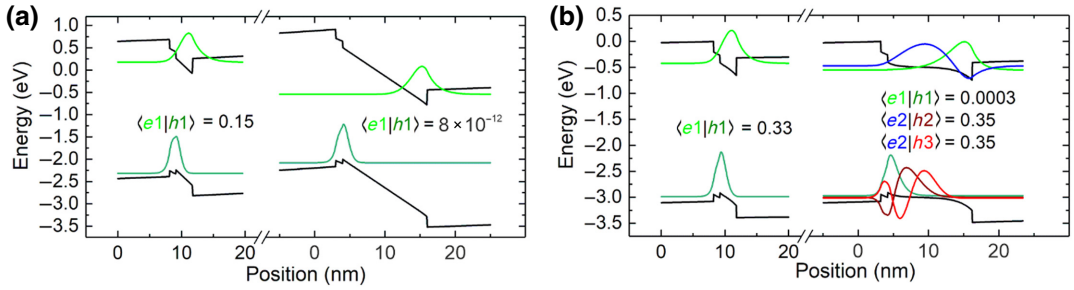

FIG. 3. Calculated band diagrams for single thin (left) and wide (right) (In, Ga)N QWs with 1-nm-thick pre-QWs (a) without and (b) under excitation. The e-h overlaps are denoted. Note that, under excitation, $e2$-$h2$ and $e2$-$h3$ transitions dominate in wide QWs.

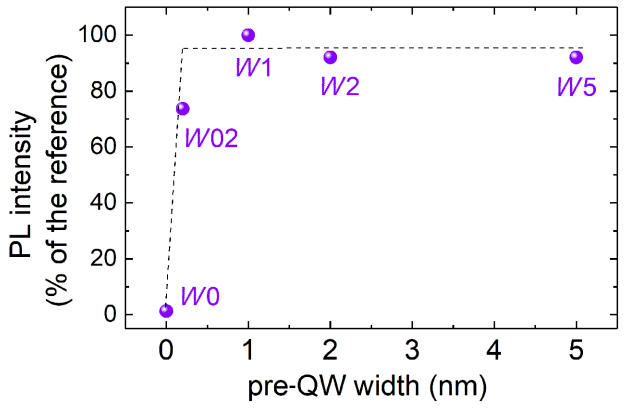

FIG. 4. Relative PL intensity of 12-nm-thick QW structures as a function of pre-QW thickness. Dashed lines are shown to guide the eye.

QW, where $\langle\psi_e|\psi_h\rangle$ is high for the standard and staggered structures. In the case of the third series, with 12-nm-wide QWs, we observe that the impact of the pre-QW on the wave-function overlap is negligible.

Two selected cases that illustrate the $A1$ and $W1$ samples are presented in Fig. 3. Energy-band structures and respective $\langle\psi_e|\psi_h\rangle$ in thin and thick QWs with a 1-nm-thick pre-QW without and under excitation ($j = 100$ A/cm^2) are plotted. One can see that the observed emission from wide QWs comes from the excited states $e2$-$h2$ and $e2$-$h3$ [see Fig. 3(b)], while the wave-function overlap between the ground states is negligible.

The impact of the width of the pre-QW layer is investigated in the series $W0$-$W5$ with a variable pre-QW thickness, d, from 0 to 5 nm. The 12-nm-thick QWs are intentionally used and compared in this experiment to analyze and contrast the results with the 2.6-nm-thick QWs. A summary of the PL intensity with respect to pre-QW thickness is presented in Fig. 4, while details of the peak wavelength position are listed in Table I. Surprisingly, for standard wide QWs (sample $W0$), we observe the lowest PL intensity. The situation is dramatically changed for staggered thick QWs ($W02$-$W5$). The PL intensity measured for the structures with a pre-QW is significantly higher than that of the standard one. The highest PL intensity of all is recorded for the staggered QW structure, $W1$, and it is taken as the reference intensity for all other samples. What is interesting is that the growth of one monolayer of an intermediate-In-content pre-QW results in a dramatic increase of PL, and an increase in pre-QW thickness does not bring further significant improvement in intensity. We also grown other QWs with In contents of 22%–24% (results not shown) without a pre-QW layer, and for all these samples, the result is similar, i.e., very weak PL. Since the built-in fields in the 12-nm-wide QWs do not impact the luminescence intensity as much as in the 2.6-nm-wide counterparts, we can conclude that the pre-QW plays an important role in reducing nonradiative-recombination centers, which are most likely related to point defects or other structural defects.

As can be seen, there is a strong improvement in the PL intensity, even if a monolayer-thick pre-QW is used, and there is no more improvement for wider pre-QW thickness. This provides evidence that the pre-QW layer is not acting in the same way as an (In, Ga)N underlayer used in MOCVD-grown LEDs, which is used to "bury" defects originating during the growth of high-temperature GaN in MOCVD. In the case of the underlayer used in the MOCVD-grown LEDs, monolayer-thick (In, Ga)N is insufficient to bury the defects and there is an improvement with the thickness of the (In, Ga)N underlayer, which we do not observe in case of the pre-QW.

For staggered QWs, we have an indium content of 8% before the QW and 16% and 24% in the QW; therefore, the In composition change is about 8 percentage points at each interface. For standard QWs, the In content is 8% before the QW and 24% in the QW, resulting in an In content difference of 16 percentage points. Perhaps it is a key factor that can change the growth mechanism of efficient QWs. Below, we demonstrate that the density of nonradiative-recombination centers and other related structural defects is greatly reduced for staggered QWs.

B. Cathodoluminescence studies

To gain an insight into the origins of differences in PL intensity between standard QWs and their staggered counterparts, we investigate the thin double QW structures by cathodoluminescence (CL) imaging at room temperature. Monochromatic maps recorded at the peak QW wavelength are collected for samples $A0$, $A1$, $B0$, and $B1$. Peak wavelengths observed in CL differ slightly from the

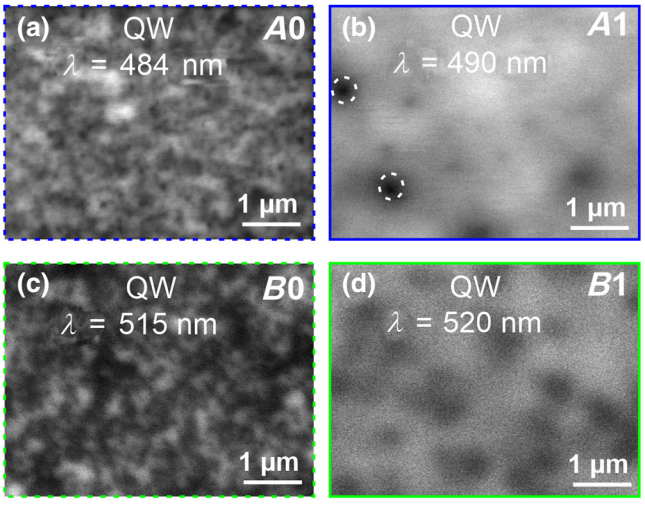

FIG. 5. CL monochromatic maps of (a) $A0$, (b) $A1$, (c) $B0$, and (d) $B1$ samples taken at wavelengths corresponding to QW emission.

ones measured by PL due to different excitation powers. Figures 5(a)–5(d) compare the CL results for samples *A*0, *A*1, *B*0, and *B*1, respectively. Two of the dark spots present in Fig. 5(b), marked in circles, are also observed in the CL map collected at $\lambda = 365$ nm (map is not presented here), which suggests that these defects are not generated during growth of the QW but rather originate from the GaN substrate. Two conclusions can be drawn from the analysis of the CL maps shown in Fig. 5. First, comparing the emission from the QWs of samples *A*0 and *A*1, we see that the number of dark spots and their density is much lower for the staggered QW (*A*1) presented in Fig. 5(b) than that for the standard QW (*A*0) presented in Fig. 5(a). The same observation holds for *B*0 and *B*1 samples, for which the peak-emission mapping showed a more uniform emission from the staggered QW (*B*1) than that from the standard counterpart (*B*0), cf. Figs. 5(d) and 5(c), respectively. Second, by comparison of sample *A*0 to *B*0 and *A*1 to *B*1, we see that the higher the In content of the QW, the higher the density of dark spots in the CL maps, both for standard and staggered QWs. The CL results show clearly that the decrease in PL for high-In-content QWs is related to the generation of defects. A reduction of these defects through insertion of the pre-QW increases the homogeneity of the emission observed in CL and significantly increases the PL intensity. The density of the dark spots seen in CL for *A*1 and *B*1 samples is relatively low when compared to the *A*0 and *B*0 counterparts, so, to confirm whether the dark spots have the same or different origins, dedicated TEM studies would be needed.

C. Identification of defects by TEM

Selected samples are studied by cross-section TEM to investigate the presence of extended defects: two samples without a pre-QW, *B*0 and *W*0, and one sample with a 2-nm pre-QW, *W*2. The cross-section studies of samples *B*0 and *W*0 confirm the presence of long BSFs in the QWs. The

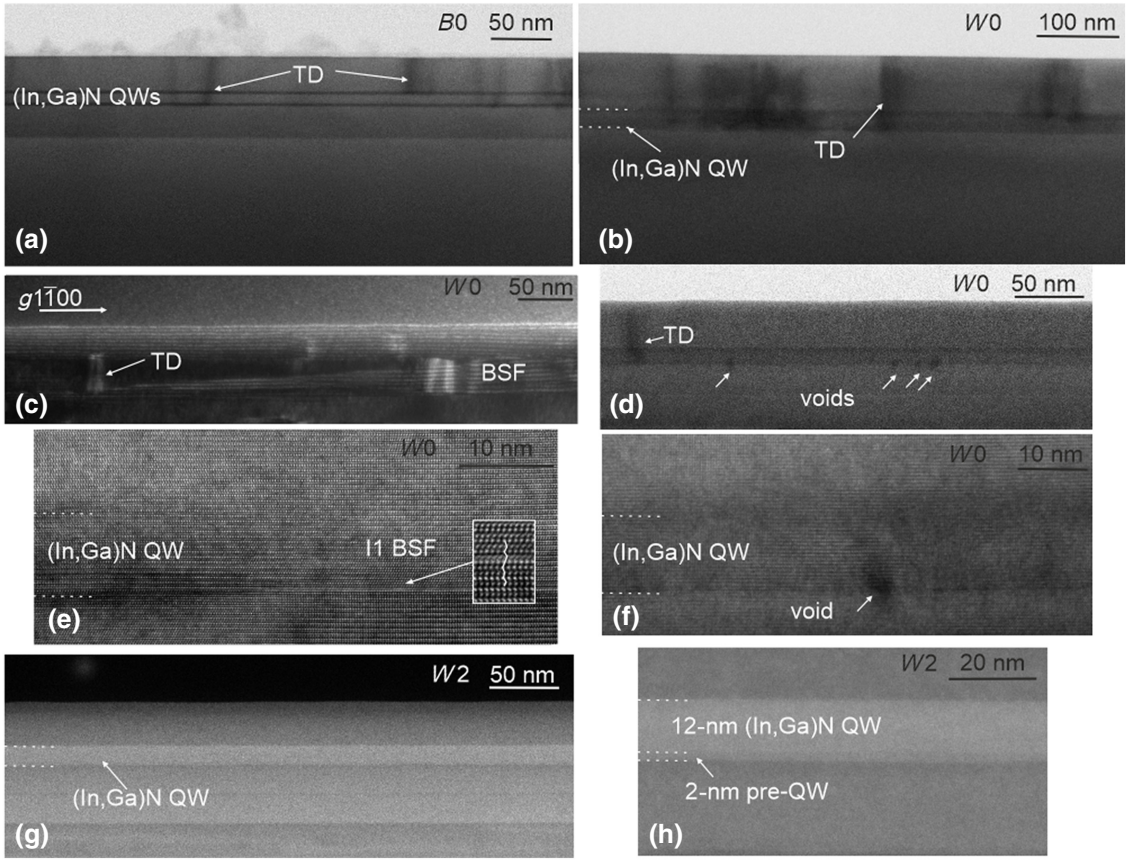

FIG. 6. Cross-section TEM images of samples *B*0 and *W*0 evidencing the presence of defects in the (In, Ga)N QWs. (a),(b) BF STEM images of sample *B*0 and *W*0, respectively. TDs starting from the QWs are indicated. (c) Dark-field TEM image of the *W*0 structure taken with *g*1–100, showing a long BSF in the QW and TDs starting at the BSF. (d) HRTEM image taken along the [11−20] zone axis of the *W*0 structure, showing the *I*1 BSF at the bottom of the QW; stacking sequence of the basal 0002 planes across the BSF is indicated in the inset. (e) BF STEM image of the *W*0 sample, showing voids present at the lower interface of the QW with the barrier. (f) HRTEM image of the *W*0 sample taken along the [11−20] zone axis, showing the roundish area of lower intensity caused by strain due to the void present at the lower QW interface. (g),(h) HAADF STEM images of structure *W*2; no structural defects are observed in the field of view.

BF STEM images presented in Figs. 6(a) and 6(b) show numerous threading dislocations (TDs) starting from the QWs. The dark-field two-beam investigation of such areas with TDs shows that the dislocations originate from BSFs formed in the QW, cf. Fig. 6(c). The observed TDs are geometrically necessary dislocations formed at the folds of prismatic-stacking-fault (PSF) domains terminating the BSFs. The mechanism for the formation of TDs from BSF plus PSF domains is described elsewhere [23,24]. The $I1$ BSFs are repeatedly found to form at the bottom interface between the (In, Ga)N barrier and high-In-content QW layer, as shown in the high-resolution TEM image in Fig. 6(d). Except for the BSFs and TDs, we also find voids present at the bottom interface of the (In, Ga)N QW in the $W0$ structure. The presence of voids is manifested by the local roundish features caused by the strain due to empty space in the crystal lattice, as marked with arrows in Figs. 6(e) and 6(f) and additionally marked with an arrow in Fig. 6(f). Similar features are observed for thermally annealed (In, Ga)N QWs, in which structural degradation is initiated by the formation of voids, caused by agglomeration of vacancies diffusing to the QWs during annealing at temperatures, on average, 200 °C higher that the growth temperature of the QW [25]. The presence of voids in the annealed (In, Ga)N QWs is accompanied by the formation of long $I1$ BSFs, indicating the same origin of both defects. The classic model for the formation of $I1$ BSFs assumes removal of one basal plane caused by the agglomeration of vacancies [14], and the only possible way to form voids in the studied QW structures is by the agglomeration of vacancies. Since the studied structures are not annealed and the growth temperatures for the MBE technique are too low to activate the diffusion of vacancies, it is more plausible that the agglomeration of point defects takes place during the abrupt change of the In composition from 8% to 22% or from 8% to 24%. Note that all the observed defects, voids, BSFs, and TDs, originate at the bottom interface of the QW, where the composition difference between layers is the highest. The last two TEM pictures presented in Figs. 6(g) and 6(h) show HAADF STEM images of the $W2$ structure. In this case, no structural defects, such as TDs, BSFs, or voids, are visible, which is consistent with the high PL intensity observed for this QW. In Fig. 6(h), magnification of the wide QW of the $W2$ sample shows that a 2-nm pre-QW is formed during epitaxy, as intended.

D. Application of pre-QW concept in laser diodes

As shown above, the pre-QW is successfully used to increase the efficiency of cyan and green active regions. Blue-light emitters, such as laser diodes [26], which rely on a slightly lower In content of around 15%–17%, are not found to be affected by growing intermediate (In, Ga)N composition before the QW. To show an operational device based on an active region grown in the same way as sample $W1$, we present a laser diode operating at 487 nm. L-I-V and emission spectra for the device under continuous-wave operation at room temperature are presented in Fig. 7. The results presented indicate a huge improvement in the threshold current density, compared to a previous report [15], and prove the applicability of the concept investigated in the current work.

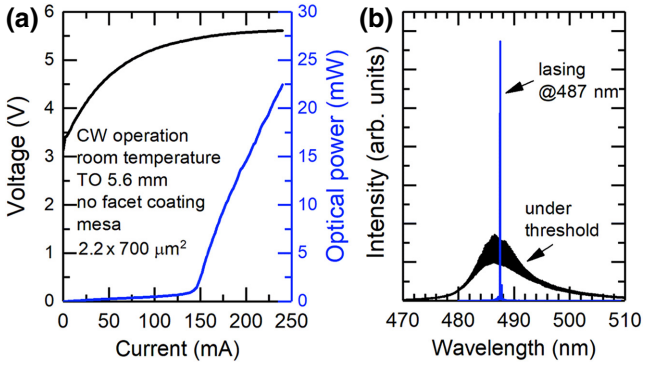

FIG. 7. (a) L-I-V characteristics of the cyan laser diode under continuous-wave operation at room temperature. (b) High-resolution emission spectra below and above the threshold. Results are obtained for no facet coating in a standard TO-can 5.6 mm.

IV. DISCUSSION

Higher quantum efficiency of staggered QWs in reference to the standard rectangular-composition-profile counterparts is usually explained by a reduction of the electric field. However, we observe an increase in PL intensity for staggered QWs, even with a lower overlap of electron-hole wave functions. Therefore, there has to be an additional strong Shockley-Read-Hall (SRH) nonradiative-recombination channel present in standard QWs, such as structural defects. We experimentally demonstrate high-density dark spots for QWs without pre-QWs; this is an indication of the defects responsible for SRH nonradiative recombination. For samples with pre-QWs, CL is very uniform. Confirming the presence of point defects in the QWs is very challenging and usually indirect. However, the formation of defects at the bottom interface of high-In-content QWs is corroborated by TEM, where voids, BSFs, and TDs are found only in the samples without pre-QWs. The formation of such structural defects requires a large number of vacancies. Therefore, we attribute quenching of the PL to the presence of a large number of vacancies in QWs for the structures without pre-QWs. Growth of the pre-QW of an intermediate indium content between the barrier and the well prevents the generation of vacancies, leading, as a result, to a large increase of the PL intensity.

V. CONCLUSIONS

We show that staggered QWs grown by PAMBE have higher luminescence intensity compared to standard rectangular-composition-profile QWs. In our work, we study standard and staggered constructions for two thicknesses of QWs: 2.6 and 12 nm. The study provides evidence of the consequence of the application of thin pre-QWs on the luminescence and structural properties of QWs. We demonstrate an additional unexpected benefit of staggered QWs, namely, improved optical quality that is not solely a result of higher wave-function overlap. When a pre-QW layer of an intermediate In composition is inserted below the QW, point-defect formation is reduced, and therefore, the optical quality of the staggered QW is higher. Standard-QW CL shows a high dark-spot density. TEM studies provide evidence for the presence of voids, BSFs, and TDs at the bottom interface of the QW that are believed to be formed through the aggregation of point defects. The presented CL and TEM results support the hypothesis that the use of pre-QWs of an intermediate In content leads to a reduction of point-defect density, which, in turn, is responsible for an increase of the nonradiative-recombination rate. A lower number of nonradiative-recombination centers explains the increased quantum efficiency reported for staggered QWs. The applicability of the pre-QW concept is presented for a CW 487-nm operational laser diode.

ACKNOWLEDGMENTS

The authors would like to thank Grzegorz Staszczak for CL measurements and Marcin Kryśko for XRD measurements. This work receives funding from the Foundation for Polish Science cofinanced by the European Union under the European Regional Development Fund within the TEAM-TECH POIR.04.04.00-00-210C/16-00 and POWROTY/REINTEGRATION POIR.04.04.00-00-4463/17-00 projects. This work is also financially supported by the National Science Centre Poland within SONATA Grants No. 2019/35/D/ST5/02950 and No. 2019/35/D/ST3/03008. The research leading to these results also receives funding from the Norway Grants 2014-2021 via the National Centre for Research and Development within Grant No. NOR/SGS/BANANO/0164/2020 and from the National Centre for Research and Development Grants No. LIDER/29/0185/L-7/15/NCBR/2016, No. LIDER/35/0127/L9/17/NCBR/2018, and No. LIDER/287/L-6/14/NCBR/2015.

[1] V. Fiorentini, F. Bernardini, F. Della Sala, A. Di Carlo, and P. Lugli, Effects of macroscopic polarization in III-V nitride multiple quantum wells, Phys. Rev. B **60**, 8849 (1999).

[2] M. Auf der Maur, A. Pecchia, G. Penazzi, W. Rodrigues, and A. Di Carlo, Efficiency Drop in Green InGaN/GaN Light Emitting Diodes: The Role of Random Alloy Fluctuations, Phys. Rev. Lett. **116**, 027401 (2016).

[3] Y. Wang, B. Duan, G. Deng, Y. Yu, Y. Niu, J. Yu, H. Ma, Z. Shi, B. Zhang, and Y. Zhang, The study of properties of blue-green InGaN/GaN multiple quantum wells grown at different pressures, Superlattices Microstruct. **153**, 106863 (2021).

[4] A. David, N. G. Young, C. A. Hurni, and M. D. Craven, Quantum Efficiency of III-Nitride Emitters: Evidence for Defect-Assisted Nonradiative Recombination and Its Effect on the Green Gap, Phys. Rev. Appl. **11**, 031001 (2019).

[5] H. Turski, M. Siekacz, Z. R. Wasilewski, M. Sawicka, S. Porowski, and C. Skierbiszewski, Nonequivalent atomic step edges—role of gallium and nitrogen atoms in the growth of InGaN layers, J. Cryst. Growth **367**, 115 (2013).

[6] M. Siekacz, MŁ Szańkowska, A. Feduniewicz-Zmuda, J. Smalc-Koziorowska, G. Cywiński, S. Grzanka, Z. R. Wasilewski, I. Grzegory, B. Łucznik, S. Porowski, and C. Skierbiszewski, InGaN light emitting diodes for 415–520 nm spectral range by plasma assisted MBE, Phys. Status Solidi C **6**, S917 (2009).

[7] M. Siekacz, M. Sawicka, H. Turski, G. Cywiński, A. Khachapuridze, P. Perlin, T. Suski, M. Boćkowski, J. Smalc-Koziorowska, M. Kryśko, *et al.*, Optically pumped 500 nm InGaN green lasers grown by plasma-assisted molecular beam epitaxy, J. Appl. Phys. **110**, 063110 (2011).

[8] P. M. F. J. Costa, R. Datta, M. J. Kappers, M. E. Vickers, C. J. Humphreys, D. M. Graham, P. Dawson, M. J. Godfrey, E. J. Thrush, and J. T. Mullins, Misfit dislocations in In-rich InGaN/GaN quantum well structures, Phys. Status Solidi A **203**, 1729 (2006).

[9] R. Liu, J. Mei, S. Srinivasan, H. Omiya, F. A. Ponce, D. Cherns, Y. Narukawa, and T. Mukai, Misfit dislocation generation in InGaN epilayers on free-standing GaN, Jpn. J. Appl. Phys. **45**, L549 (2006).

[10] Y. Chen, C. Haller, W. Liu, S. Y. Karpov, J.-F. Carlin, and N. Grandjean, GaN buffer growth temperature and efficiency of InGaN/GaN quantum wells: The critical role of nitrogen vacancies at the GaN surface, Appl. Phys. Lett. **118**, 111102 (2021).

[11] J.-X. Shen, D. Wickramaratne, C. E. Dreyer, A. Alkauskas, E. Young, J. S. Speck, and C. G. Van de Walle, Calcium as a nonradiative recombination center in InGaN, Appl. Phys. Express **10**, 021001 (2017).

[12] R. A. Arif, Y.-K. Ee, and N. Tansu, Polarization engineering via staggered InGaN quantum wells for radiative efficiency enhancement of light emitting diodes, Appl. Phys. Lett. **91**, 091110 (2007).

[13] H. Li, P. Li, J. Kang, Z. Li, Y. Zhang, Z. Li, J. Li, X. Yi, J. Li, and G. Wang, Quantum efficiency enhancement of 530 nm InGaN green light-emitting diodes with shallow quantum well, Appl. Phys. Express **6**, 052102 (2013).

[14] D. Hull and D. J. Bacon, in *Introduction to Dislocations*, edited by D. Hull and D. J. Bacon (Butterworth-Heinemann, Oxford, 2011), 5th ed. pp. 157–169.

[15] H. Turski, G. Muziol, P. Wolny, S. Grzanka, G. Cywiński, M. Sawicka, P. Perlin, and C. Skierbiszewski, Cyan laser

diode grown by plasma-assisted molecular beam epitaxy, Appl. Phys. Lett. **104**, 023503 (2014).

[16] C. Skierbiszewski, H. Turski, G. Muziol, M. Siekacz, M. Sawicka, G. Cywiński, Z. R. Wasilewski, and S. Porowski, Nitride-based laser diodes grown by plasma-assisted molecular beam epitaxy, J. Phys. D: Appl. Phys. **47**, 073001 (2014).

[17] M. Siekacz, A. Feduniewicz-Żmuda, G. Cywiński, M. Kryśko, I. Grzegory, S. Krukowski, K. E. Waldrip, W. Jantsch, Z. R. Wasilewski, S. Porowski, and C. Skierbiszewski, Growth of InGaN and InGaN/InGaN quantum wells by plasma-assisted molecular beam epitaxy, J. Cryst. Growth **310**, 3983 (2008).

[18] G. Muziol, H. Turski, M. Siekacz, P. Wolny, S. Grzanka, E. Grzanka, P. Perlin, and C. Skierbiszewski, Enhancement of optical confinement factor by InGaN waveguide in blue laser diodes grown by plasma-assisted molecular beam epitaxy, Appl. Phys. Express **8**, 032103 (2015).

[19] G. Muziol, H. Turski, M. Siekacz, P. Wolny, J. Borysiuk, S. Grzanka, P. Perlin, and C. Skierbiszewski, Aluminum-free nitride laser diodes: Waveguiding, electrical and degradation properties, Opt. Express **25**, 33113 (2017).

[20] SiLENSe 6.4 package, https://str-soft.com/devices/silense/

[21] G. Muziol, H. Turski, M. Siekacz, K. Szkudlarek, L. Janicki, M. Baranowski, S. Zolud, R. Kudrawiec, T. Suski, and C. Skierbiszewski, Beyond quantum efficiency limitations originating from the piezoelectric polarization in light-emitting devices, ACS Photonics **6**, 1963 (2019).

[22] G. Muziol, M. Hajdel, M. Siekacz, K. Szkudlarek, S. Stanczyk, H. Turski, and C. Skierbiszewski, Optical properties of III-nitride laser diodes with wide InGaN quantum wells, Appl. Phys. Express **12**, 072003 (2019).

[23] J. Smalc-Koziorowska, J. Moneta, P. Chatzopoulou, I. G. Vasileiadis, C. Bazioti, Ø Prytz, I. Belabbas, P. Komninou, and G. P. Dimitrakopulos, The heterogeneous nucleation of threading dislocations on partial dislocations in III-nitride epilayers, Sci. Rep. **10**, 17371 (2020).

[24] I. G. Vasileiadis, I. Belabbas, C. Bazioti, J. Smalc-Koziorowska, P. Komninou, and G. P. Dimitrakopulos, Stacking fault manifolds and structural configurations of partial dislocations in InGaN epilayers, Phys. Status Solidi B **258**, 2100190 (2021).

[25] J. Smalc-Koziorowska, E. Grzanka, A. Lachowski, R. Hrytsak, M. Grabowski, S. Grzanka, S. Kret, R. Czernecki, H. Turski, L. Marona, *et al.*, Role of metal vacancies in the mechanism of thermal degradation of InGaN quantum wells, ACS Appl. Mater. Interfaces **13**, 7476 (2021).

[26] G. Muziol, H. Turski, M. Siekacz, P. Wolny, M. Sawicka, S. Grzanka, P. Perlin, T. Suski, Z. R. Wasilewski, I. Grzegory, *et al.*, True-blue laser diodes grown by plasma-assisted MBE on bulk GaN substrates, Phys. Status Solidi C **11**, 666 (2014).